ORIGINAL ARTICLE

Precision Positioning with Shape-Memory-Alloy Actuators

Kai-Hung Liang, Kuo-Han Kao, and Szu-Chi Tien*

Department of Mechanical Engineering, National Cheng Kung University, Taiwan

(**Received** 24 June 2013; **Accepted** 3 September 2013; **Published on line** 1 December 2013)

*Corresponding author: sctien@mail.ncku.edu.tw

DOI: 10.5875/ausmt.v3i4.209

Abstract: The primary purpose of this study is to improve the positioning performance of shape-memory-alloy (SMA) actuators. In order to achieve this goal, the system nonlinearity was reduced with the inversion of a nonlinear model. The system could then be approximated with a linear model. It is easy to construct the corresponding model-reference-adaptive-system (MRAS) based on this linear model. Experimental results show that the MRAS is robust with respect to external disturbances and improves the positioning performance. In addition, with the proposed control scheme, the simulation results will closely match experimental results, which is useful to predict the system performance at the controller-design stage.

Keywords: Adaptive control; hysteresis compensation; model reference adaptive system; precision positioning; shape memory alloy

1. Introduction

Shape Memory Alloys (SMAs) have the ability to recover a predetermined shape through the application of heat, even after a large strain occurs [1]. In addition, SMAs have been used broadly in different applications due to many features such as durability, low noise during operation, a simple mechanism for energy transformation, high power-to-weight ratio, and being innocuous for living bodies [1-4]. For example, in aeronautic engineering SMAs can be used to control the opening area of an exhaust nozzle on a gas turbine [5], reducing the system weight since they have a high power-to-weight ratio compared to conventional actuators. In civil engineering, SMAs can be integrated with other passive, semi-active, or active components, in order to reduce damage caused by environmental impact due to their high damping capacity, durability, and fatigue resistance [6]. In the case of bioengineering, SMAs have been used in prostheses [7-9] and surgeries [4, 10] due to their lightweight, dexterous, and biologically innocuous properties.

Although SMAs have many superior features in comparison to other materials or actuators, they are often difficult to control due to high nonlinearity and sensitivity to variations of the ambient temperature [11]. Therefore, in order to enhance the performance of SMAs, the development of good models and the application of suitable control schemes are two issues to be studied.

In order to describe the characteristics of SMAs, a variety of constitutive models have been developed [12, 13]. These constitutive models feature physical insights of SMAs since each parameter has a physical meaning. However, they often consist of complicated mathematical equations and may require many experiments to determine each parameter. In contrast to modeling, many control schemes were studied and applied to control SMAs to improve the performance. In the cases of simple adaptive control (SAC) and sliding mode control for instance, they increase the system robustness against modeling uncertainties and external disturbances [14-16]. Other control schemes, for example a PID (proportional-integral-derivative) controller combined with fuzzy logic [17] and neural-network-based controllers [18] were utilized to

cope with the nonlinearity of SMAs; all of them provided good choices to control SMAs.

In this article, the nonlinearity of SMAs is modeled with the Preisach model [19, 20] instead of constitutive models. Although the Preisach model is constructed by fitting experimental hysteresis curves which do not directly relate to material properties (i.e. the Preisach model provides fewer insights into the mechanism controlling the material transformation), it still reflects the hysteretic behavior and is convenient for simulation and control applications [21-23]. Therefore, the nonlinearity of SMAs was initially reduced using the inverse-Preisach-model-based control [24, 25], allowing the new system to be approximated with a linear model. It is simple to construct the corresponding model-reference-adaptive-system (MRAS) [26] based on this linear model to cope with modeling uncertainties and external disturbances. In addition, it is expected that the simulation will closely match the experimental results since the inverse-Preisach-model-based control will transform the SMAs system to approach a linear system used for constructing the MRAS. This feature is useful to predict the system performance at the controller-design stage.

The remainder of this article is organized as follows. The material and method used in this research are covered in Sec. 2. The experimental results and discussions are given in Sec. 3. Conclusions are presented in Sec. 4.

Kai-Hung Liang received the B.S. degree in system and naval mechatronic engineering from National Cheng Kung University, Taiwan, in 2009 and the M.S. degree in mechanical engineering from National Cheng Kung University, Taiwan, in 2011.
His research is about identifying, modeling SMA, and applying control schemes to SMA to compensate for errors caused by hysteresis, limited bandwidth and modeling uncertainties. In addition, he focuses on achieving precision positioning and tracking of SMA such that SMA can be used as actuators on applications like micro-manipulator or mimetic hands.

Kuo-Han Kao received the B.S. degree in mechanical and electromechanical engineering from National Sun Yat-sen University, Taiwan, in 2010, the M.S. degree in mechanical engineering from National Cheng Kung University, Taiwan, in 2012.
He is an engineer in Gallant Precision Machining Co., Ltd. His research interests are SMA-actuated biomimetic hand and visual servo control. Now, he focuses on integrating CCD systems to capture images of panels and coding image processing algorithms to do dimensional measurement or defect detection.

Szu-Chi Tien received the B.S. degree in naval architecture from National Taiwan University, Taiwan, in 1995, the M.S. degree in mechanical engineering from National Cheng Kung University, Taiwan, in 1997, and the Ph. D. degree in mechanical engineering from University of Washington, US, 2007.
He is an assistant professor in the Mechanical Engineering Department at National Cheng Kung University, Taiwan, and his research interests are system identification, system modeling, mechanism analysis, and controller design. In particular, he focuses on utilizing smart materials for achieving precision positioning and tracking; results are applied on precision alignment, inspection, manufacturing and biomimetic fields.

2. Material and Method

2.1. Experiment Setup

Figure 1 shows the schematic diagram of the experimental setup. A nickel-titanium SMA-wire (diameter $\phi = 150\mu m$; typical contraction time $T_c = 1s$; typical relaxation time $T_r = 2s$; manufactured by Dynalloy Inc.) fixed to the SMA-holder with pre-tension F_i of $3N$ (measured with a load cell, SMT S-type, Interface Inc.) was constructed. Varying the applied voltage on the SMA-wire, allows its length to change and be recorded with a linear-variable-differential transformer (LVDT) (JEC-AG DC-DC, Honeywell Inc.).

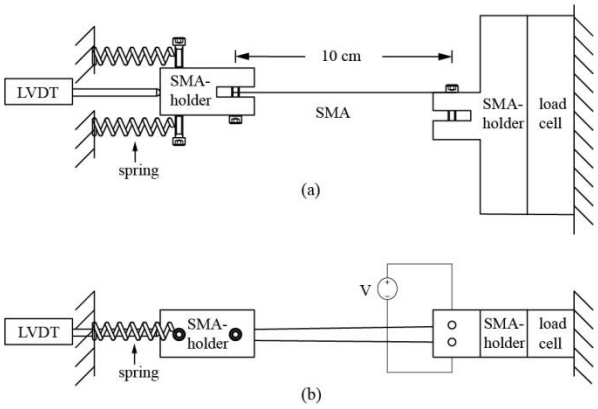

Figure 1. Schematic diagram of the experimental setup. (a) Is the top view and (b) is the side view.

Remark 1. *In this research, the maximum deformation ratio and the maximum applied voltage for the SMA are limited to 4% (i.e., 4mm) and 4V, respectively. This is based on the recommended operating conditions provided by the manufacturer.*

2.2. Control Schemes

As shown in Figure 2(a), the SMA-wire was modeled as two cascaded sub-systems: hysteresis H and linear dynamics G. The control strategy of this research is to (i) utilize an inverse hysteresis model H_0^{-1} to reduce the system's nonlinearity in order to model it as a linear model G_0, and (ii) construct an MRAS based on a reference model G_m such that the adaptive controller C_{adp} can make the deformation of SMA d_{SMA} equal the output of the reference model d_m (see Figure 2(b)). The detailed procedures are elaborated in the following two subsections.

2.2.1. Preisach-model-based control

In this research, the nonlinear hysteresis is modeled using the Preisach model [19] and the deformation of the SMA $d_{SMA}(t)$ can be described using the integral of all weighted Preisach hysterons,

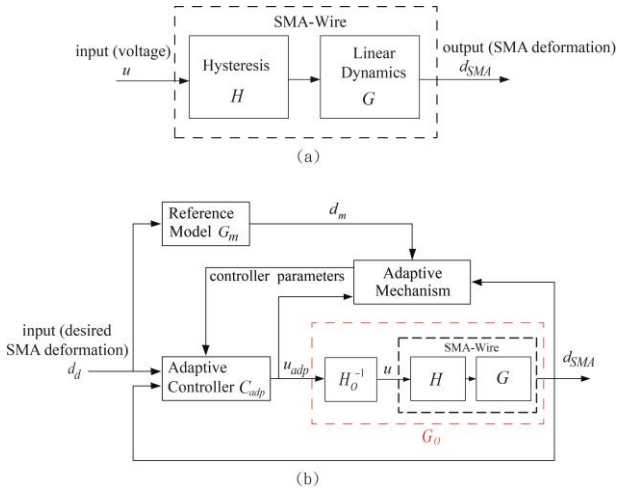

Figure 2: The conceptual explanation depicting the SMA-system (plot (a)) and the combination of the hysteresis-compensation and MRAS in this research (plot (b)).

$$d_{SMA}(t)=\int\int_{\alpha\geq\beta}\mu(\alpha,\beta)\gamma_{\alpha\beta}[u(t)]d\alpha d\beta\,, \tag{1}$$

where $\mu(\alpha,\beta)$ is a weighting function in the Preisach model, and $\gamma_{\alpha\beta}[u(t)]$ is the Preisach hysteron whose on-off state is determined by the input voltage $u(t)$.

In order to identify the weighting function $\mu(\alpha,\beta)$, the Preisach plane needs to be considered in a discrete form [27], i.e., Eq. (1) needs to be expressed as,

$$d_{SMA}(t)=\sum_{k=1}^{n}\gamma_k\mu_k A_k\,, \tag{2}$$

where γ_k is the discrete Preisach hysteron which has a value of "1" for the on-state or "0" for the off-state, A_k represents the k^{th} area in the discretized Preisach plane, and μ_k is the weighting function for area A_k.

As an example, Figure 3, shows a four interval case (i.e. $N=4$) where the total number, n, of the discrete areas in the Preisach plane is ten (i.e., $n=\frac{N(N+1)}{2}$), and the corresponding deformation at time t_1, t_2, and t_3 are,

$$\begin{aligned} d_{SMA}(t_1)&=\sum_{i=1}^{10}\mu_i A_i\,,\\ d_{SMA}(t_2)&=\sum_{i=1}^{6}\mu_i A_i+\sum_{i=8}^{10}\mu_i A_i\,,\\ d_{SMA}(t_3)&=\sum_{i=1}^{3}\mu_i A_i+\sum_{i=5}^{6}\mu_i A_i+\sum_{i=9}^{10}\mu_i A_i\,. \end{aligned} \tag{3}$$

Therefore, by applying a test input u (the input shown in Figure 3(d)) and mapping the input-to-output relation experimentally as,

$$[d_{SMA}]\approx[\psi][\eta]\,, \tag{4}$$

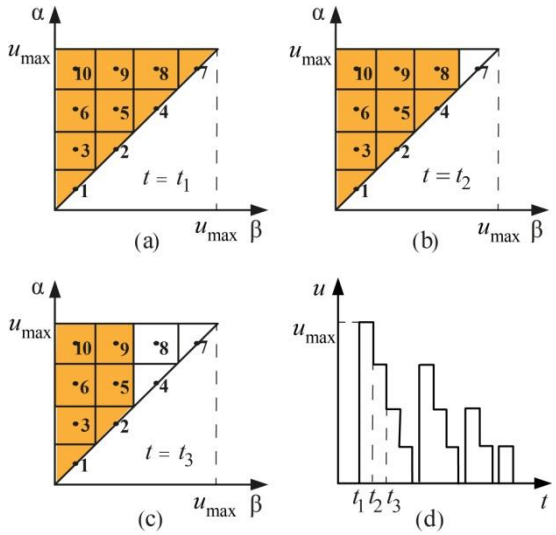

Figure 3. A ten-partition example of the Preisach plane (the colored areas represent the "switched on" hysterons). Plots (a) to (c) show the states of the Preisach plane corresponding to the test input u shown in plot (d) when $t=t_1$~t_3.

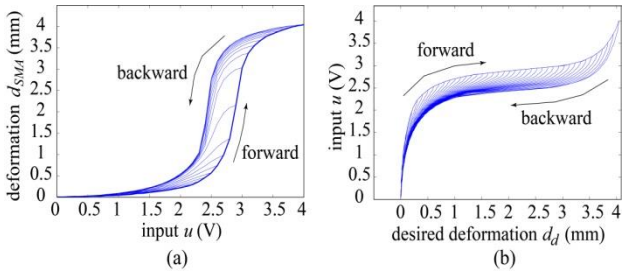

Figure 4. The constructed hysteresis model H_0 (plot (a)) and inverse hysteresis model H_0^{-1} (plot (b)) of our SMA.

the weighting function μ_k can be obtained from $[\eta]$ by solving Eq. (4) using the least-squares method [25], where $[d_{SMA}]$ is the vector of the measured output (i.e., SMA deformation), $[\eta]$ is the vector of the weighting function μ_K multiplied by the known area A_k, and $[\psi]$ is the hysteron matrix consisting of the on-state and off-state (i.e., 1 or 0). The hysteresis model H_0 constructed is shown in Figure 4(a).

Similarly, the inverse hysteresis can be modeled using the same concept since the inverse hysteresis curve and the hysteresis curve are symmetric with respect to $d_{SMA}=u$. In other words, the inverse hysteresis can be considered as a kind of hysteretic effect which exchanges the input with output. Therefore, rather than conducting any experiment, the inverse hysteresis model H_0^{-1} can be constructed through interpolation of the input-to-output relation of H_0 and deriving the "new" weighting function μ_k (the result is shown in Figure 4(b)).

2.2.2. Adaptive control

In this research, adaptive control based on MRAS is used to compensate for the modeling uncertainties and external disturbances. In particular, the MIT rule [26] is

utilized and the MRAS shown in Figure 2(b) can be converted to the overall control block diagram of Figure 5. It should be noted that given a reference model G_m, the goal of the MIT rule is to make the system output d_{SMA} equal the output of the reference model d_m. The process can be elaborated as follows.

The definition of a cost function $J(\theta)$ in terms of the error e is

$$J(\theta) \triangleq \frac{1}{2}(e)^2 = \frac{1}{2}(d_{SMA} - d_m)^2, \tag{5}$$

which means the time derivative J of is,

$$\dot{J} = \frac{dJ}{dt} = \frac{\partial J}{\partial \theta}\frac{d\theta}{dt} = e\frac{\partial e}{\partial \theta}\dot{\theta}, \tag{6}$$

where $\theta = [\theta_1, \theta_2]$ is the adjustable parameter. In order to make the error e approach zero, the time derivative of θ can be designed with a positive constant λ

$$\dot{\theta} = -\lambda e\frac{\partial e}{\partial \theta}, \tag{7}$$

such that Eq. (6) becomes,

$$\dot{J} = -\lambda\left(e\frac{\partial e}{\partial \theta}\right)^2 \le 0, \tag{8}$$

i.e., the cost function J will decrease as long as error e is non-zero.

Given the reference model $G_m = \dfrac{b_m}{s+am}$ and the nominal model $G_0 = \dfrac{b}{s+a}$ as shown in Figure 5, the system output d_{SMA} and the reference output d_m can be expressed as,

$$\frac{d(d_{SMA})}{dt} = -ad_{SMA} + bu_{adp}, \tag{9}$$

$$\frac{d(d_m)}{dt} = -a_m d_m + b_m d_d, \tag{10}$$

If the control law is set to be,

$$u_{adp} = \theta_1 d_d - \theta_2 d_{SMA}, \tag{11}$$

Eq. (9) can be rewritten as,

$$\frac{d(d_{SMA})}{dt} = -(a + b\theta_2)d_{SMA} + b\theta_1 d_d, \tag{12}$$

Therefore, by inspecting Eq. (10) and Eq. (12), two equations will be identical by setting the adjustable parameter θ to be,

$$\theta_1 = \frac{b_m}{b} \triangleq \theta_{1,pft}, \tag{13}$$

$$\theta_2 = \frac{a_m - a}{b} \triangleq \theta_{2,pft}, \tag{14}$$

which is called perfect model-following, where $\theta_{1,pft}$ and $\theta_{2,pft}$ are the corresponding values.

Finally, the error sensitivity with respect to the adjustable parameter (defined as $\partial e/\partial\theta$) can be approximated with the perfect model-following condition,

$$\frac{\partial e}{\partial \theta_1} = \frac{b}{p + a + b\theta_2}d_d \approx \frac{b}{p + a_m}d_d, \tag{15}$$

$$\frac{\partial e}{\partial \theta_2} = \frac{-b^2\theta_1}{(p + a + b\theta_2)^2}d_d \approx \frac{-b}{(p + a_m)}d_{SMA}, \tag{16}$$

where $p \triangleq d/dt$. Substitution of Eqs. (15) and (16) into Eq. (7) gives the time derivative of the adjustable parameter

$$\frac{d\theta_1}{dt} = -\lambda e\frac{\partial e}{\partial \theta_1} = -\gamma\left(\frac{a_m}{p + a_m}d_d\right)e, \tag{17}$$

$$\frac{d\theta_2}{dt} = -\lambda e\frac{\partial e}{\partial \theta_2} = -\gamma\left(\frac{a_m}{p + a_m}d_{SMA}\right)e, \tag{18}$$

where $\gamma = \lambda b / a_m$ is the adaptation gain. This completes the control structure shown in Figure 5.

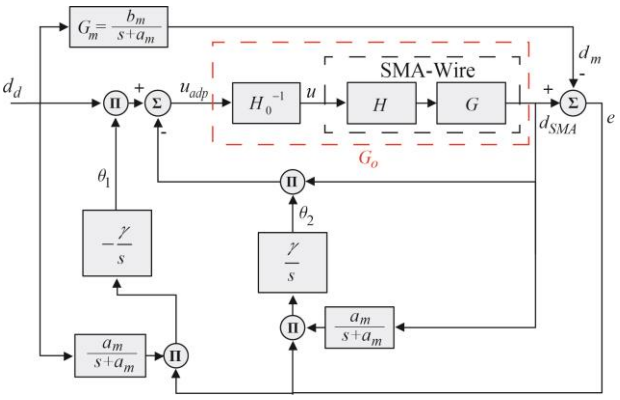

Figure 5. Control block diagram of the SMA-wire.

Remark 2. *In practice, once the SMA system is linearized to G_0 (see Figure 5), any robust feedback controller (even a simple PID-controller) can be added to the control-loop to improve the performance. However, the MRAS-controller utilized in this research is designed in the Lyapunov-stability sense regardless of the modeling uncertainties and external disturbances. Therefore, it is expected to exhibit greater robustness. In the worst case the model G_0 may deviate from the real system G significantly and saturation on the input u_{adp} may occur. The error e will not vanish in this case.*

3. Experimental results and discussions

3.1. Hysteresis compensation

The hysteresis of the system can be compensated with the inverse hysteresis model H_0^{-1} and using the procedure shown in Sec. 2.2.1. In other words, given a desired deformation of SMA d_d, the input to compensate for the hysteresis can be calculated as,

$$u = H_0^{-1}(d_d). \tag{19}$$

As shown in Figure 6(b), before compensation, the SMA-wire shows high nonlinearity; after compensation, the nonlinearity is reduced substantially.

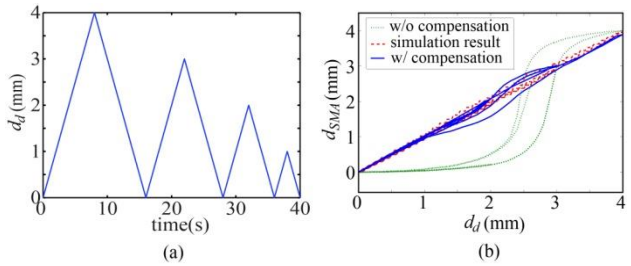

Figure 6. Hysteresis compensation. (a) The desired deformation of SMA d_d in the time domain, and (b) comparison of the hysteretic effect (dotted line: without compensation; dashed line: simulation result with inverse-hysteresis-model compensation; solid line: experimental result with inverse-hysteresis-model compensation).

Remark 3. *The quantization errors from discrete formulation of the hysteresis model can be analyzed by increasing the partition number N until the quantization error levels off [28]. In this research, we set* $N = 40$ *to maintain accuracy and minimize computational expense.*

3.2. Linear dynamics compensation

Since the system's nonlinearity has been reduced with the inverse hysteresis model H_0^{-1}, the linear dynamic model G_0 can be obtained from the frequency response of a sine-sweep test. At first, a desired deformation of SMA d_d in a sine-wave form is set as the input. The corresponding voltage to compensate for the hysteretic effect is then calculated via Eq.(19) and applied to the SMA to measure the deformation of SMA d_{SMA} (i.e., the output). Therefore, by constantly varying the frequency of the sine-wave and analyzing the corresponding input-output relation, the linear dynamic model G_0 can be obtained. It can be seen from Figure 7 that the measured system is similar to a first-order system with a bandwidth of around $0.1Hz$. Therefore, G_0 is set by curve-fitting,

$$G_0(s) = \frac{b}{s+a} = \frac{0.74}{s+0.74}. \tag{20}$$

Further, in order to increase the bandwidth of the system, the reference model G_m is set to have a bandwidth of $0.5Hz$,

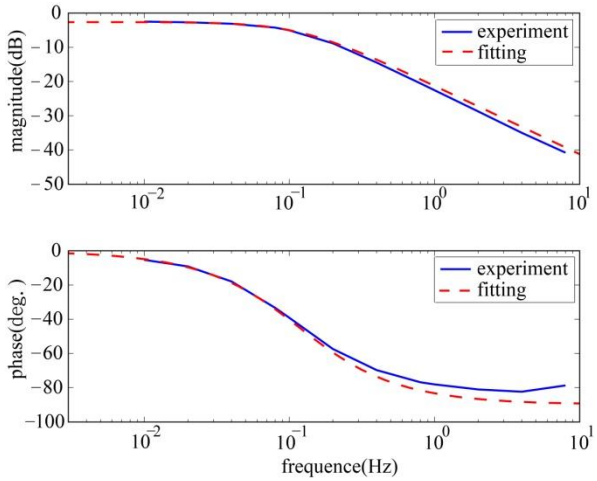

Figure 7. The Bode plot of the linear dynamics of the SMA-wire.

$$G_m(s) = \frac{b_m}{s+a_m} = \frac{3.14}{s+3.14}. \tag{21}$$

Once the model G_m and G_0 are determined, the adaptive control scheme shown in Sec. 2.2.2 can be implemented. In particular, to reduce the time in which error e tends to zero, the initial value of the adjustable parameter $\theta_i(0)$ is set to be the value $\theta_{i,pft}$ (see Eqs. (13) and (14)) in the so-called "perfect model-following" condition [26],

$$\theta_1(0) = \theta_{1,pft} = \frac{b_m}{b} = \frac{3.14}{0.74} = 4.24, \tag{22}$$

$$\theta_2(0) = \theta_{2,pft} = \frac{a_m - a}{b} = \frac{3.14 - 0.74}{0.74} = 3.24. \tag{23}$$

Moreover, the rise time, settling time, and overshoot with respect to different adaptation gains γ are evaluated in simulation. It can be seen from Figure 8 that when the adaptation gain γ equals one, the system has the shortest settling time and a relatively small rise time and overshoot. Therefore, γ is set to one in our experiment (the result is shown in Figure 9).

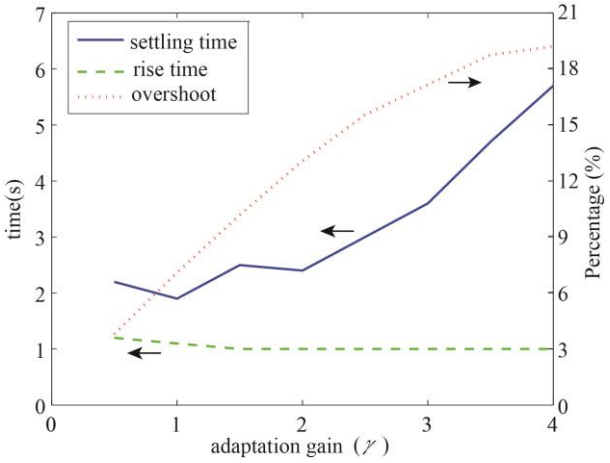

Figure 8. Simulation results of three performance measures with respect to adaptation gains γ.

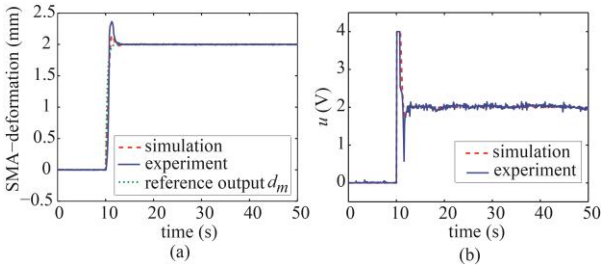

Figure 9. Comparison of the positioning results after integrating the inverse-Preisach-model-based control and adaptive control (i.e., the proposed control scheme shown in Figure 5). (a) Output comparison, and (b) input comparison. (It should be noted that the adaptation gain $\gamma = 1$, desired deformation of SMA $d_d = 2mm$, and a $4V$ input-saturation is set in both the simulation and experiment).

Inspection of the simulation and the experimental results highlights two issues:

Reducing the nonlinearity of a system helps the experimental results closely match the simulation. Since the nonlinearity of the SMA-wire is reduced with the hysteresis compensation (see Figure 6), a linear model G_0 can describe the system sufficiently and thus increase the accuracy of the performance-prediction at the simulation stage. As shown in Figure 9, the simulation and experimental results are similar with the exception of the overshoot which may occur due to modeling errors and external disturbances.

Setting the initial value of the adjustable parameter $\theta(0)$ based on the perfect-following condition may reduce the time in which the error e tends to zero. It is noted that, as long as the criterion of Eq. (8) is satisfied, the error e will eventually tend to zero. In other words, the initial value of the adjustable parameter $\theta(0)$ can be set arbitrarily (usually zero). However, if there is no modeling error (i.e., G_0 describes our system perfectly), the perfect-following condition shown in Eqs. (22) and (23) provide a good choice. It can be seen from Figure 10 that, even under modeling error, the adjustable parameters $\theta_{1,\text{exp}}$ and $\theta_{2,\text{exp}}$ in the experimental results approach our initial settings.

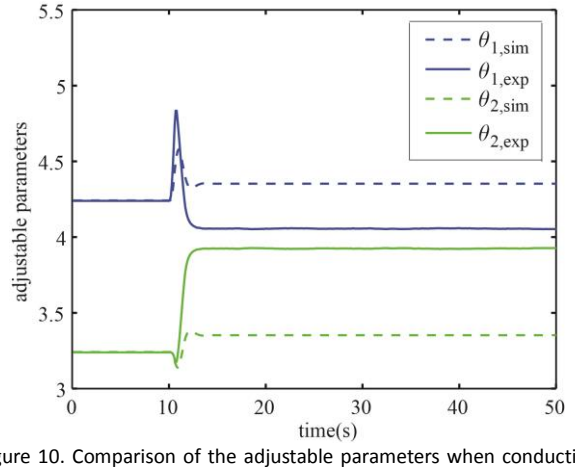

Figure 10. Comparison of the adjustable parameters when conducting the positioning task shown in Figure 9. (Dashed line: simulation results; solid line: experimental results).

4. Conclusion

In this article a control scheme for integrating system-nonlinearity-reduction and MRAS is proposed and demonstrated via a positioning example with an SMA-wire. The experimental results demonstrated the MRAS robustness to external disturbance and improving the positioning performance. In addition, using the proposed control scheme, the simulation results will closely match the experimental results, which is useful to predict the system performance at the controller-design stage. In the future, a model to capture the difference of dynamics when heating and cooling a SMA will be studied. The proposed scheme may further improve the positioning performance using this new model, and be extended to additional SMA-actuated applications such as micro-manipulator and mimetic hands.

5. Acknowledgement

The support from the National Science Council (Republic of China) on Grant NSC 101-2221-E-006-187 is gratefully acknowledged.

References

[1] E. H. Schiller, "Heat engine driven by shape memory alloys: Prototyping and design," M. S. Thesis, Virginia Polytechnic Institute and State University, 2002.
Available: http://scholar.lib.vt.edu/theses/available/etd-09252002-170731/unrestricted/ETD.pdf

[2] A. Falvo, "Thermo mechanical characterization of nickel-titanium shape memory alloys," phd dissertation, Mechanical Engineering, University Della Calabria, Italy, 2007.

[3] S. G. Wax and R. R. Sands, "Electroactive polymer actuators and devices," in *Proceedings of SPIE 3669*, Newport Beach, CA, USA, 1999, pp. 2-10.
doi: 10.1117/12.349666

[4] S. P. Hannula, O. Söderberg, T. Jämsä, and V. K. Lindroos, "Shape memory alloys for biomedical applications," *Advances in Science and Technology,* vol. 49, pp. 109-118, 2006.
doi: 10.4028/www.scientific.net/AST.49.109

[5] G. Song, N. Ma, H. J. Lee, and S. Arnold, "Design and control of a proof-of-concept variable area exhaust nozzle using shape-memory alloy actuators," *Smart Materials and Structures,* vol. 16, no. 4, pp. 1342-1347, 2007.
doi: 10.1088/0964-1726/16/4/048

[6] G. Song, N. Ma, and H. N. Li, "Applications of shape memory alloys in civil structures," *Engineering Structures,* vol. 28, no. 9, pp. 1266-1274, 2006.
doi: 10.1016/j.engstruct.2005.12.010

[7] K. J. De Laurentis and C. Mavroidis, "Mechanical design of a shape memory alloy actuated prosthetic hand," *Technol Health Care,* vol. 10, no. 2, pp. 91-106, 2002.

[8] M. Bergamasco, F. Salsedo, and P. Dario, "Shape memory alloy micromotors for direct-drive actuation of dexterous artificial hands," *Sensors and Actuators,* vol. 17, no. 1–2, pp. 115-119, 1989. doi: 10.1016/0250-6874(89)80071-X

[9] K. Kuribayashi, "A new actuator of a joint mechanism using tini alloy wire," *International Journal of Robotics Research,* vol. 4, no. 4, pp. 47-58, 1986. doi: 10.1177/027836498600400404

[10] N. B. Morgan, "Medical shape memory alloy applications—the market and its products," *Materials Science and Engineering: A,* vol. 378, no. 1–2, pp. 16-23, 2004. doi: 10.1016/j.msea.2003.10.326

[11] N. M. Lohan, L. G. Bujoreanu, and C. Baciu, "Influence of temperature variation rate on calorimetric response during heating and on martensite structure obtained after subsequent cooling of cu-zn-al shape memory alloy," *Micro & Nano Letters,* vol. 7, no. 6, pp. 540-543, 2012. doi: 10.1049/mnl.2012.0049

[12] L. C. Brinson and M. S. Huang, "Simplifications and comparisons of shape memory alloy constitutive models," *Journal of Intelligent Material Systems and Structures,* vol. 7, no. 1, pp. 108-114, 1996. doi: 10.1177/1045389X9600700112

[13] V. Birman, "Review of mechanics of shape memory alloy structures," *Applied Mechanics Reviews,* vol. 50, no. 11, pp. 629-645, 1997. doi: 10.1115/1.3101674

[14] M. Kumon, I. Mizumoto, Z. Iwai, and A. Indou, "Shape memory alloy actuator with simple adaptive control," *International Journal of Innovative Computing, Information and Control,* vol. 4, no. 12, pp. 429-429, 2007. doi: 10.1109/ICICIC.2007.519

[15] G. Song, B. Kelly, and B. N. Agrawal, "Active position control of a shape memory alloy wire actuated composite beam," *Smart Materials and Structures,* vol. 9, no. 5, pp. 711-716, 2000. doi: 10.1088/0964-1726/9/5/316

[16] J. R. Hill, K. W. Wang, and J.-H. Roh, "Position control of shape memory alloy actuators with load and frequency dependent hysteresis characteristics," in *Proceeding SPIE 7286*, San Diego, California, USA, 2009, pp. 728609-728609-728609. doi: 10.1117/12.815627

[17] K. K. Ahn and N. B. Kha, "Modeling and control of shape memory alloy actuators using preisach model, genetic algorithm and fuzzy logic," *Mechatronics,* vol. 18, no. 3, pp. 141-152, 2008. doi: 10.1016/j.mechatronics.2007.10.008

[18] E. Asua, V. Etxebarria, and A. García-Arribas, "Neural network-based micropositioning control of smart shape memory alloy actuators," *Engineering Applications of Artificial Intelligence,* vol. 21, no. 5, pp. 796-804, 2008. doi: 10.1016/j.engappai.2007.07.003

[19] F. Preisach, " ber die magnetische nachwirkung," *Zeitschrift für Physik,* vol. 94, no. 5-6, pp. 277-302, 1935. doi: 10.1007/BF01349418

[20] M. A. Krasnosel'skiĭ and A. V. Pokrovskii, *Systems with hysteresis*. Berlin; New York: Springer-Verlag, 1989.

[21] F. Li, J. Q. Mao, H. S. Ding, W. B. Zhang, H. B. Xu, and C. B. Jiang, "A new method to identify the preisach distribution function of hysteresis," *Materials Science Forum,* vol. 475-479, pp. 2107-2110, 2005. doi: 10.4028/www.scientific.net/MSF.475-479.2107

[22] A. Ktena, D. I. Fotiadis, P. D. Spanos, and C. V. Massalas, "A preisach model identification procedure and simulation of hysteresis in ferromagnets and shape-memory alloys," *Physica B: Condensed Matter,* vol. 306, no. 1–4, pp. 84-90, 2001. doi: 10.1016/S0921-4526(01)00983-8

[23] D. Hughesy and J. T. Wenz, "Preisach modeling of piezoceramic and shape memory alloy hysteresis," *Smart Materials and Structures,* vol. 6, no. 3, pp. 287-300, 1997. doi: 10.1088/0964-1726/6/3/007

[24] R. V. Iyer and T. Xiaobo, "Control of hysteretic systems through inverse compensation," *IEEE Control Systems,* vol. 29, no. 1, pp. 83-99, 2009. doi: 10.1109/MCS.2008.930924

[25] X. Tan, R. Venkataraman, and P. S. Krishnaprasad, "Control of hysteresis: Theory and experimental results," in *Proceeding SPIE 4326*, Newport Beach, CA, USA 2001, pp. 101-112. doi: 10.1117/12.436463

[26] K. J. Astrom and B. Wittenmark, *Adaptive control*: Pearson Education Taiwan Ltd, 2006.

[27] K. K. Leang, "Iterative learning control of hysteresis in piezo-based nano-positioners: Theory and application in atomic force microscopes," PhD dissertation, University of Washington, 2004. Available: http://www.kam.k.leang.com/academics/pubs/KamKLeangPhDDec2004.pdf

[28] P. J. Ko, Y. P. Wang, and S. C. Tien, "Inverse-feedforward and robust-feedback control for high-speed operation on piezo-stages," *International Journal of Control,* vol. 86, no. 2, pp. 197-209, 2012. doi: 10.1080/00207179.2012.721568